

1 ***In silico*-guided optimisation of oxygen gradients in hepatic spheroids**

2 Joseph Leedale¹, Helen E. Colley², Harriet Gaskell³, Dominic P. Williams⁴, Rachel N. Bearon¹,

3 Amy E. Chadwick³, Craig Murdoch², Steven D. Webb^{1,5*}

4 ¹EPSRC Liverpool Centre for Mathematics in Healthcare, Dept. of Mathematical Sciences,
5 University of Liverpool, Liverpool, L69 7ZL, UK

6 ²School of Clinical Dentistry, University of Sheffield, Claremont Crescent, Sheffield, S10
7 2TA, UK

8 ³MRC Centre for Drug Safety Science, Dept. of Molecular and Clinical Pharmacology,
9 University of Liverpool, Liverpool, L69 3GE, UK

10 ⁴AstraZeneca, IMED Biotech Unit, Drug safety & Metabolism, Cambridge Science Park,
11 Cambridge, CB4 0FZ, UK

12 ⁵Dept. of Applied Mathematics, Liverpool John Moores University, Liverpool, L3 3AF, UK

13

14 ***Correspondence**

15 Dr Steven D. Webb
16 Dept. of Applied Mathematics
17 Liverpool John Moores University
18 Liverpool L3 3AF
19 United Kingdom
20 Tel: +44 (0)151 231 2217
21 Email: S.D.Webb@ljmu.ac.uk
22

23 **E-mail addresses:**

24 j.leetdale@liverpool.ac.uk (JL); h.colley@sheffield.ac.uk (HEC); hgaskell@uic.edu (HG);

25 dominic.p.williams@astrazeneca.com (DPW); rbearon@liverpool.ac.uk (RNB);

26 aemercer@liverpool.ac.uk (AEC); c.murdoch@sheffield.ac.uk (CM); S.D.Webb@ljmu.ac.uk

27 (SDW).

28 **Abstract**

29 One of the key advantages of assessing the hepatotoxic potential of xenobiotics in spheroids
30 rather than monolayer cell culture is the existence of a more physiologically relevant testing
31 environment. Three-dimensional cultures support spatial gradients in nutrients such as oxygen
32 that can be exploited to better represent *in vivo* gradients that exist along a fundamental sub-
33 unit of liver microarchitecture, the liver sinusoid. The physical and physiological processes that
34 result in the establishment of such gradients can be described mathematically. Quantification
35 of the rates governing these processes and optimisation of cell culture conditions can be
36 performed *in silico* to better inform experimental design. In this study, we take into account
37 cell line-specific physiological properties, spheroid size and the impact of experimental
38 equipment geometries in order to demonstrate how mathematical models can be optimised to
39 achieve specific *in vivo*-like features in different scenarios. Furthermore, the sensitivity of such
40 optimised gradients is analysed with respect to culture conditions and considerations are given
41 to prevent the emergence of hypoxic regions in the spheroid. The methodology presented
42 provides an enhanced understanding of the mechanisms of the system within this simulated *in*
43 *vitro* framework such that experimental design can be more carefully calibrated when
44 conducting experiments using hepatic spheroids.

45 **Keywords:** Liver spheroids; HepG2; HepaRG; Hypoxia; Oxygen gradient; In silico modelling.

46 1 Introduction

47 Two-dimensional (2D) cell culture systems have been extensively used to enhance our
48 understanding of human biology with applications ranging from the study of pathophysiology
49 at the cellular level to the pharmacology and toxicology of novel drugs. However, there remains
50 a considerable disparity between *in vitro* experimental findings and *in vivo* relevance,
51 motivating the need for improved *in vitro* methods. The enhanced physiological relevance of
52 three-dimensional (3D) *in vitro* models provides an important link between 2D *in vitro* models
53 and *in vivo* whole-body biology (Yamada & Cukierman, 2007). While many 3D model
54 systems, from scaffold-based models to microfluidic bioreactors, are now being employed to
55 increase translational applicability, the use of spheroid models in particular has become
56 progressively important to fundamental medical research and safety assessment (Kyffin et al.,
57 2018). 3D spheroids represent a convenient and versatile *in vitro* model that improves
58 physiological relevance, cell morphology and functionality (compared to 2D systems), yet are
59 simple to deploy, cost-effective and amenable to higher throughput techniques. Although these
60 systems inevitably lack certain physiological complexities (e.g. vasculature) as a consequence
61 of their relative simplicity, other features such as *in vivo*-like gradients can be established with
62 the move to three dimensions. Of paramount importance in these physiological gradients is
63 oxygen.

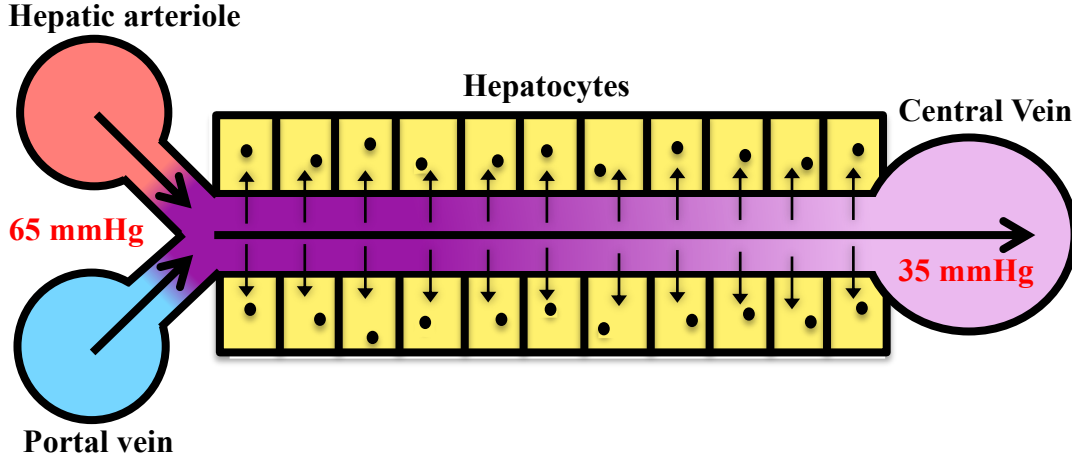
64 Physiological oxygen gradients are a prime example of homeostasis within healthy cells and
65 tissues and significant disruption to oxygen availability can lead to apoptosis and necrosis.
66 Hypoxia is a prevalent feature in the growth stages of solid tumours due to the rapid growth
67 characteristic of mutated cancer cells causing an abnormal distribution of cells and nutrient-
68 supplying blood vessels (Vaupel et al., 1989, Muz et al., 2015). As cancer cells typically
69 proliferate more rapidly than normal cells, a tumour mass is soon formed that is unable to be
70 adequately supplied by the surrounding vasculature, that also tends to be immature and poorly

71 formed. A hypoxic region is formed in the centre of the tumour due to the distance between the
72 oxygen supply and this core of cells. This process is symptomatic of an early-stage tumour,
73 otherwise known as an avascular tumour, as the tumour has not yet induced the production of
74 its own blood vessel network (Brown & Giaccia, 1998, Riffle & Hegde, 2017). Similarly,
75 hyperoxic conditions can lead to the generation of reactive oxygen species and oxidative stress,
76 and thus there exists a bounded range of oxygen tensions that is functionally optimal for each
77 tissue (Carreau et al., 2011, Lee et al., 2014). Avascular tumours are studied experimentally by
78 culturing cancer cells as spheroids as they share similar growth kinetics (Freyer, 1988, Grimes
79 et al., 2016). The avascular phase of the life cycle of a tumour covers the initial mutations of
80 normal cells through to a diffusion-limited steady state where the tumour's growth is limited
81 by a balance between nutrient consumption and nutrient supply via diffusion. Mathematical
82 modelling can facilitate the refinement and optimisation of *in vitro* studies to more accurately
83 translate these results to a more physiologically realistic *in vivo* scenario (Williams et al., 2013).
84 The importance of understanding the local environment and mechanisms within tumour
85 spheroids to develop medical applications has led to considerable mathematical modelling
86 efforts in this area. Some work has focused on reproducing growth and development processes
87 (Chaplain, 1996, Grimes et al., 2016), while others investigate the effects of various oxygen
88 consumption kinetics in different geometries and hypoxic environments (Grimes et al., 2014b,
89 Grimes et al., 2014a, Leedale et al., 2014). Acknowledgement of the importance of spatial
90 dynamics in spheroids has also led to mathematical models that simulate 3D pharmacological
91 processes such as drug delivery and metabolism (Ward & King, 2003, Mehta et al., 2012).

92 The spatial heterogeneity, or zonation, observed in tumours is a key characteristic that must be
93 addressed when modelling these systems. These spatial features are also an essential
94 characteristic of other physiological environments such as the primary detoxification system
95 of the body, the liver, and in particular the hepatic lobule and liver sinusoid (Jungermann &

96 Kietzmann, 2000). The spatial gradients that exist within the sinusoid microenvironment
97 impact upon overall hepatocyte function, metabolic capabilities and susceptibility to toxins
98 with respect to location (Lee-Montiel et al., 2017). Therefore, cellular spheroids provide
99 effective *in vitro* tools to study the pharmacological and toxicological effects of drugs in the
100 liver throughout the local microenvironment by replicating physiologically relevant features
101 within these 3D structures.

102 The oxygen gradient is a key characteristic of the liver sinusoid that must be maintained in
103 spheroids in order to preserve this *in vivo*-like zonation (Figure 1), which ranges from 65
104 mmHg in the periportal region of the sinusoid to 35 mmHg at the central vein (Jungermann &
105 Keitzmann, 1996, Jungermann & Kietzmann, 2000). The oxygen gradient is primarily
106 dependent on the supply of oxygen, flow rate, length of sinusoid and cellular uptake. For *in*
107 *vitro* spheroid models that do not include flow, their size can theoretically be optimised in order
108 to recapitulate the same range of oxygen concentrations from boundary to core. This range
109 would then provide the appropriate environment to make the test system more comparable
110 when studying effects of cell function and spatial variation in metabolism between periportal
111 and perivenous (centrilobular) regions. Indeed, the role of the oxygen gradient in regulating
112 metabolic zonation is critically important for pharmacological studies, whether or not this
113 regulation is direct or via downstream signalling (Kietzmann, 2017). The supply of oxygen *in*
114 *vitro* is dependent on the externally controlled atmosphere, type and volume of culture media
115 (which can be controlled *in vitro*), and diffusion of oxygen through the media and spheroid.
116 The length of sinusoid, which is assumed to be constant and regular *in vivo*, is effectively
117 represented by the radius of the *in vitro* spheroid. All of these parameters that determine the
118 hepatic oxygen gradient *in vitro* can be optimised using a suitable mathematical model.



119

120 Figure 1: A schematic representation of the liver sinusoid. Mixed blood from the portal vein
 121 and the oxygen-carrying hepatic arteriole flows towards the central vein where it is drained
 122 from the liver lobule. As blood flows from the periportal region to the perivenous
 123 (centrilobular) region, oxygen is removed from the blood by hepatocytes establishing an
 124 oxygen gradient ranging from 65 mmHg (periportal) to 35 mmHg (perivenous).
 125

126 2 Materials and methods

127 2.1 Model derivation

128 2.1.1 Model I: Spheroid only

129 The mathematical model of spatiotemporal oxygen dynamics throughout the spheroid includes
 130 diffusion and oxygen uptake terms in a continuum approach. We assume that oxygen
 131 consumption is dependent on the local oxygen concentration in a non-linear manner such that
 132 the consumption rate saturates for higher oxygen levels. Therefore, we describe the oxygen
 133 dynamics within the spheroid using the following partial differential equation (PDE):

$$\frac{\partial C}{\partial t} = D_1 \nabla^2 C - \frac{V_{max} C}{C + K_m}, \quad \mathbf{x} \in \Omega. \quad (1)$$

134 Oxygen concentration (mol/m^3) is represented by C , D_1 is the diffusion rate constant in m^2/s
 135 (assumed to be independent of radial position), V_{max} is the maximum consumption rate in

136 mol/m³/s and K_m represents the oxygen concentration at which consumption is half maximal
 137 (mol/m³). Time is given by t while \mathbf{x} represents the spatial vector with the equation being
 138 considered within domain Ω (the spheroid). Since we will be looking at oxygen dynamics that
 139 occur on a much faster timescale than cell cycle dynamics (growth and division) we assume
 140 the radius of the spheroid to be constant, R . The system is assumed to be at steady state in a
 141 radially symmetric sphere (see Figure 2A) and is presented in spherical coordinates in equation
 142 (2) so that the problem is reduced to a 1-dimensional equation in variable r , the radial
 143 coordinate. The following system (writing the Laplacian operator with respect to the radial
 144 coordinate) is used to describe steady state spatial oxygen dynamics in a radially-symmetric
 145 sphere:

$$\frac{D_1}{r^2} \frac{\partial}{\partial r} \left(r^2 \frac{\partial C}{\partial r} \right) - \frac{V_{max} C}{C + K_m} = 0, \quad r \leq R, \quad (2)$$

$$\frac{\partial C}{\partial r} = 0, \quad r = 0. \quad (3)$$

146 The concentration of oxygen at the boundary of the sphere is fixed such that

$$C = C_R, \quad r = R. \quad (4)$$

147 Initially the oxygen concentration is given by $C(r, 0) = C_R \forall r \in \Omega$.

148 2.1.2 Model II: Spheroid in well

149 Model I requires the oxygen concentration at the spheroid boundary to be fixed at a
 150 physiologically relevant value (periportal blood/65 mmHg). However, this is difficult to
 151 calibrate *in vitro* since oxygen is not directly controlled at this region. The oxygen
 152 concentration at the boundary of a spheroid cultured *in vitro* is dependent on multiple local
 153 environmental factors such as external oxygen concentration at the air/media interface,
 154 diffusion rate of oxygen within the media, and the volume of media used. Furthermore, the

155 mathematical problem is not simply radially symmetric in 3D spherical coordinates due to the
156 geometry of the equipment used for cell culture, i.e. the physical structure of the well, and the
157 position of the spheroid. To represent these features, we have developed Model II based on the
158 *in vitro* geometry of Ultra-Low Attachment (ULA) plate wells with media (see Figure 2B).
159 Similar geometrical features are also relevant for other standard culture systems such as
160 agarose-coated 96 well plates, although these may exhibit more variation due to the formation
161 of the agarose layer. Therefore, we impose ULA plate geometry for more consistency within
162 the mathematical model simulations. Understanding the impact of culture conditions and
163 geometry on oxygen dynamics is known to be critical in order to maintain hepatocyte viability
164 and functionality *in vitro* and has previously been modelled for 2D monolayers (Yarmush et
165 al., 1992). Model II is therefore an extension of Model I used to take into account a
166 representative 3D *in vitro* environment and associated geometries.

167 Model II incorporates a realistic *in vitro* environment within the model geometry such that
168 oxygen dynamics are modelled in cylindrical coordinates with radial symmetry about the axis
169 through the centre of the well. Therefore, the steady state spatial oxygen dynamics within the
170 hepatic spheroid are governed by the following PDE:

$$\frac{D_1}{r} \frac{\partial}{\partial r} \left(r \frac{\partial C}{\partial r} \right) + D_1 \frac{\partial^2 C}{\partial z^2} - \frac{V_{max} C}{C + K_m} = 0. \quad (5)$$

171 Note that this mathematical representation could be more broadly applied to oxygen dynamics
172 in other cell-based spheroids with appropriate changes in model parameterisation. In Model II,
173 oxygen concentration in the media outside the spheroid is also considered, where there is no
174 consumption and simple diffusion governs the spatial dynamics. Oxygen diffuses at a rate, D_2 ,
175 in the outer medium and thus we have the following equation to represent oxygen dynamics
176 outside the sphere:

$$\frac{D_2}{r} \frac{\partial}{\partial r} \left(r \frac{\partial C}{\partial r} \right) + D_2 \frac{\partial^2 C}{\partial z^2} = 0, \quad (6)$$

177 Oxygen concentration is fixed at the air/media interface boundary condition, $C = C_A$, while
 178 zero-flux boundary conditions are imposed at all other boundaries of the geometry (walls of
 179 the well), i.e., $\nabla C \cdot \mathbf{n} = 0$, where \mathbf{n} is the outward-pointing unit normal vector. Initial
 180 conditions are given by $C(r, z, 0) = C_A$. In between the two phases at the boundary of the
 181 sphere, $r = R$, we assume continuity in C such that

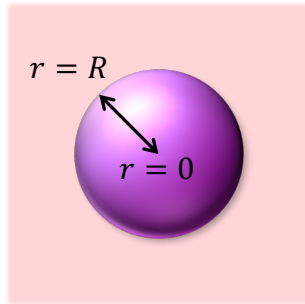
$$C_{int} = C_{ext}, \quad r = R. \quad (7)$$

182 where C_{int} here represents the concentration of oxygen at the interior of the spheroid/media
 183 interface and C_{ext} represents oxygen at the exterior. It is also assumed that the flux is equal
 184 such that mass is conserved, i.e.,

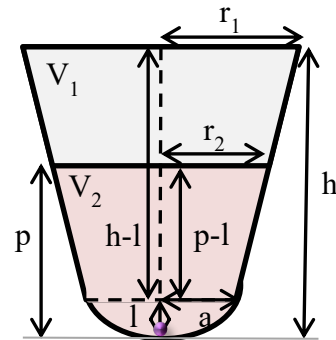
$$D_1 \frac{\partial C_{int}}{\partial r} = D_2 \frac{\partial C_{ext}}{\partial r}. \quad r = R. \quad (8)$$

185

A



B



186 Figure 2: **Model geometry schematics.** Hepatic spheroids are formed *in vitro* via media
 187 incubation whereby the hepatocytes initially seeded aggregate to form uniform spheroids. (A):
 188 Representative Model I schematic of an idealised radially symmetric spheroid. (B):
 189 Representative Model II schematic of a typical Ultra-Low Attachment (ULA) plate well with
 190 media. The oxygen concentration experienced by the cells is dependent on external
 191 concentration in the air and depth of the media. Spheroid position and environmental geometry
 192 are indicated corresponding to measurements provided in Table 1.

193

V_1	Well volume	360 μl
V_2	Media volume	100 μl
r_1	Well radius (top)	3.429 mm
h	Depth of well	11.303 mm
a	Well radius (bottom)	3.175 mm
l	Height of spherical cap	1.6 mm
r_2	Media radius (top)	3.2338 mm
p	Media depth	3.848 mm

194
 195 Table 1: Physical measurements of the geometry of a typical Ultra-Low Attachment (ULA)
 196 plate (Costar® 96-well Ultra Low Attachment (Corning Life Sciences, 2018)) with media,
 197 used to culture hepatic spheroids *in vitro* (see corresponding schematic in Figure 2B).
 198

199 2.2 Model parameterisation

200 Oxygen consumption parameters (V_{max} and K_m) for human hepatocellular cell lines were
 201 obtained using Seahorse Technology, which monitors oxygen consumption rates (OCR) and
 202 extracellular acidification rates (ECAR) in live cells to determine bioenergetic behaviour. The
 203 Seahorse experiments carried out by Kamalian et al. (2018) yielded a panel of OCR values for
 204 both HepaRG and HepG2 cell types. The maximum oxygen consumption rates (corresponding
 205 to V_{max} in the *in silico* modelling) were derived by summing the mean non-mitochondrial and
 206 maximal respiration OCR values. These rates were presented per 10,000 cells and thus an
 207 average hepatocyte volume of $3.4 \times 10^{-15} \text{ m}^3$ (Lodish et al., 2000) was used to convert OCR to
 208 the desired units for V_{max} ($\text{mol}/\text{m}^3/\text{s}$). Maximum consumption rates were therefore calculated
 209 as $V_{max} = 4.40 \times 10^{-2} \text{ mol}/\text{m}^3/\text{s}$ for HepaRG cells and $V_{max} = 1.54 \times 10^{-2} \text{ mol}/\text{m}^3/\text{s}$ for HepG2
 210 cells. It is possible that OCR measured in different cell culture conditions (2D, 3D, suspension,
 211 etc.) may cause the exact value to vary. However, it should be noted that the values used in the
 212 model appear feasible for the system and are the same order of magnitude as V_{max} values found

213 in other multicellular spheroid studies (Leedale et al., 2014, Lesher-Pérez et al., 2017). The
214 Michaelis constant appears to be more difficult to ascertain as only measurements based upon
215 rat studies have been made. For this study we use the value for primary rat hepatocytes, $K_m =$
216 $6.24 \times 10^{-3} \text{ mol/m}^3$ (Shipley et al., 2011), itself comparable to values used in other studies and
217 models, based upon rat hepatocytes cultured using a variety of methods (Buerk & Saidel, 1978,
218 Yarmush et al., 1992, Foy et al., 1994, Colton, 1995, Allen & Bhatia, 2003, Mattei et al., 2017).

219 To determine oxygen transport parameters, the rate of oxygen diffusion through the spheroid
220 was derived based on the modelling results of Leedale et al. (2014). This previous model
221 assumed linear oxygen consumption kinetics and optimised parameter values by fitting to
222 oxygen distributions in cellular spheroids, measured under various external oxygen conditions.
223 We repeated the optimisation procedure, using the same data, but for the radially symmetric
224 diffusion model with saturating uptake (identical to equations (2)), acquiring a better fit and
225 updated diffusion coefficients. The diffusion rate of oxygen inside the sphere, D_1 , was
226 estimated to be $1.60 \times 10^{-9} \text{ m}^2/\text{s}$ and the rate outside the sphere, D_2 , is $4.85 \times 10^{-9} \text{ m}^2/\text{s}$.

227 In Model I we prescribe our fixed boundary concentration to be equivalent to the concentration
228 of oxygen at the periportal region of the sinusoid, $C_R = 65 \text{ mmHg}$ ($\sim 8.6\% \text{ O}_2$). In Model II we
229 prescribe the external far-field concentration to be equivalent to atmospheric oxygen
230 concentration, i.e., $C_A = 160 \text{ mmHg}$ ($\sim 21\% \text{ O}_2$).

231 **2.3 Numerical simulation**

232 Model II PDE solutions were obtained using COMSOL Multiphysics® software. All other
233 simulations and plotted model outputs were obtained using MATLAB.

234 **2.4 Cell culture and generation and immunohistochemical staining for hypoxia**

235 The asymmetry of oxygen distribution during spheroid culture *in vitro* was motivated and
236 supported by an illustrative example of immunohistochemical staining and so we provide the
237 experimental details here for completeness. The human hypopharyngeal carcinoma cell line,
238 FaDu (American Type Culture Collection) (Rangan, 1972) were cultured in RPMI-1640
239 medium supplemented with 10% (v/v) fetal calf serum (BioSera), 2 mM L-Glutamine, 100
240 IU/ml penicillin and 100 µg/ml streptomycin (Sigma) at 37°C in 5% CO₂. Tumour spheroids
241 were generated from FaDu cells using the liquid over-layer method as previously described
242 (Colley et al., 2014). Briefly, 100 µl of 1.2 x 10⁵/ml FaDu cells were added to each well of a
243 96-well plate coated with 1.5% type V agarose (w/v in DMEM) and incubated at 37°C, 5%
244 CO₂. Medium was changed every 48 h by removing and re-placing 50% of the medium. Images
245 of MCTS were captured using a Zeiss Axiovert 200M inverted microscope fitted with a Nikon
246 AxioCam digital camera and spheroid diameter measured using Axiovision 4.6 software. For
247 visualisation of hypoxic regions, spheroids were incubated with 170 µM Hypoxyprobe
248 (Hypoxyprobe, MA) for 2 hours, washed with PBS, fixed in 4% paraformaldehyde, embedded
249 in agarose (1.5% w/v in 10% PBS-buffered formalin), histologically processed and embedded
250 in paraffin wax. Sections (5 µM) of wax-embedded spheroids were dewaxed, rehydrated and
251 endogenous peroxidase neutralised with 3% hydrogen peroxide in methanol for 20 minutes.
252 Following antigen retrieval with 1% pronase, tissue sections were blocked for 20 minutes at
253 room temperature with 3% bovine serum albumin and incubated with mouse anti-hypoxyprobe
254 monoclonal antibody for 1 h at room temperature. Secondary antibody and avidin-biotin
255 complex provided with Vectastain Elite ABC kit (Vector Laboratories) were used in
256 accordance with the manufacturer's instructions. Finally, NovaRed (Vector Laboratories) was
257 used to visualise hypoxia. Sections were counterstained with 4',6-Diamidino-2'-phenylindole
258 dihydrochloride (DAPI; Sigma) and mounted with Prolong™ Gold Antifade (Life

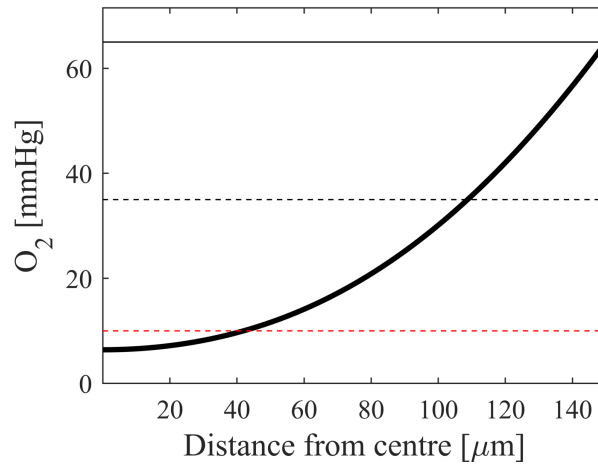
259 Technologies). Fluorescent images were captured using a spinning disc confocal microscope
260 (Olympus IX81).

261

262 **3 Results**

263 **3.1 Model I: Recapitulation of the *in vivo* sinusoid gradient by fixing the oxygen** 264 **concentration at the sphere boundary**

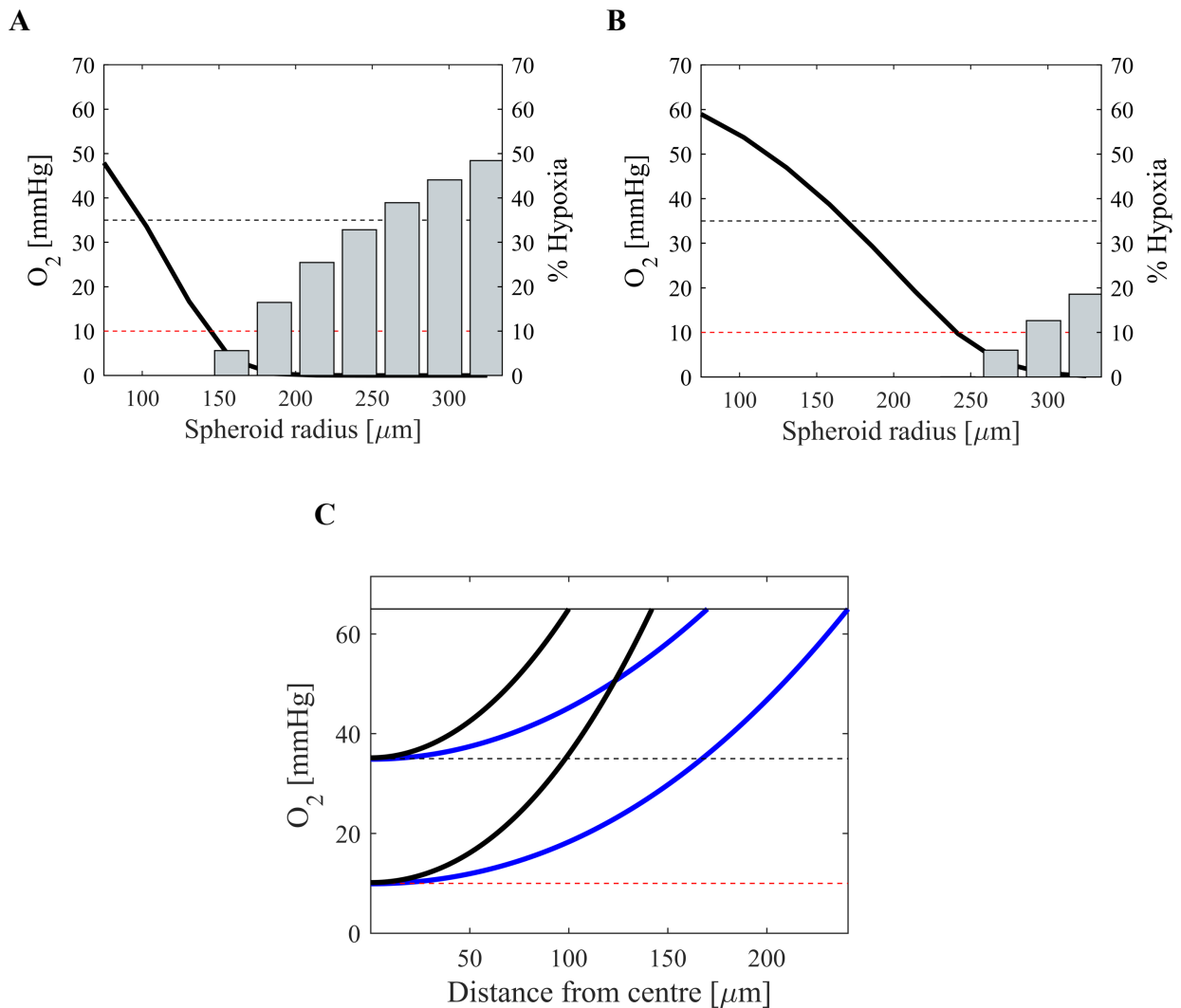
265 The steady state solution for Model I with a HepaRG spheroid radius of 150 μm and fixed
266 periportal (boundary) supply of 65 mmHg is plotted in Figure 3 such that the simulated
267 distribution of oxygen concentration across the radial distance of the spheroid at equilibrium
268 can be visualised. Physiologically relevant oxygen concentrations of oxygen within a sinusoid
269 microenvironment are indicated including desired *in vivo* oxygen values at the sinusoid
270 extrema and a value corresponding to hypoxia, defined as 10 mmHg (Martinez et al., 2008).
271 Under these conditions, the *in vivo* sinusoid gradient is not replicated with the *in silico* model
272 since there is too little oxygen present in the central region of the spheroid. This would suggest
273 that the size of the spheroid is suboptimal in this scenario and therefore the spheroid radius (R)
274 was optimised in order to ensure the relevant oxygen concentration at the spheroid core, i.e.,
275 $C(0) = 35$ mmHg.



276

277 **Figure 3: Simulation of Model I showing the spatial distribution of oxygen concentration**
 278 **at steady state in an *in silico* hepatocyte spheroid of radius 150 μm with radial symmetry.**
 279 Physiologically significant concentrations of oxygen concentration are indicated with
 280 horizontal lines representing the periportal region (black, solid), perivenous region (black,
 281 dashed) and threshold for hypoxia (red, dashed).
 282

283 Figure 4 shows how varying the radius of both HepaRG and HepG2 spheroids can be
 284 effectively implemented within the model in order to ensure that the desired oxygen gradient
 285 across the spheroid (*in silico* sinusoid) is obtained and similarly, in order to predict at what
 286 radius the spheroids are likely to experience hypoxia in the spheroid core (*in silico* central
 287 vein). HepaRG spheroids have *in vivo*-like oxygen values at the centre when they are
 288 approximately 100 μm in radius. The corresponding optimal radius for HepG2 spheroids is
 289 approximately 170 μm . Hypoxia is predicted in the spheroid interior when the radii is greater
 290 than 142 μm in HepaRG spheroids and 241 μm in HepG2 spheroids.



291 **Figure 4: Mathematical model predictions of optimal sinusoidal oxygen gradients and**
 292 **hypoxia for hepatocyte spheroids.** Oxygen concentration at the spheroid centre (i.e., “central
 293 vein”) is plotted for a range of spheroid radii (black, bold) for both HepaRG (A) and HepG2
 294 (B) cells. Physiologically relevant oxygen concentrations are denoted with horizontal lines for
 295 *in vivo* central vein oxygen concentration (black, dashed) and hypoxia (red, dashed). Grey bars
 296 represent the percentage of hepatocytes in the spheroid that are hypoxic as radii are increased.
 297 (C): Oxygen concentration profiles for optimal spheroid radii and hypoxic spheroid radii are
 298 plotted against the radial distance from the spheroid centre for both HepaRG (black) and
 299 HepG2 (blue), with physiologically relevant concentrations denoted.
 300

301 Whereas HepaRG simulations appear realistic in terms of the often cited ~150 μm oxygen
 302 diffusion distance, the estimated size at which HepG2 spheroids begin to suffer central hypoxia
 303 appears to be quite large (Carmeliet & Jain, 2000, Glicklis et al., 2004, Anada et al., 2012).
 304 However, it should be noted that there is evidence that different cell types have different
 305 metabolic demands (Olive et al., 1992) and therefore, all else being equal, it is expected that

306 optimal spheroid size should in fact vary with a variation in oxygen consumption kinetics, as
307 governed by the physical processes described in our mechanistic model. We are not aware of
308 any exact measurements of local pO_2 in HepG2 spheroids but it has been shown that HepG2
309 cells consume oxygen at a much lower rate than primary hepatocytes (Nyberg et al., 1994).
310 Furthermore, our definition of hypoxia ($C < 10$ mmHg) may be overly prescriptive compared
311 to other studies, e.g. 40 mmHg (Curcio et al., 2007), and we do not account for other
312 environmental factors (i.e., pH, glucose, etc.) or cell death as indicators for limitations in
313 spheroid size - only the physical processes of oxygen diffusion and consumption. In light of
314 these considerations we opt to carry out the rest of our investigation based on the HepaRG cell
315 line to focus on the impact of well geometry on oxygen dynamics in the *in vitro* spheroid
316 system, but stress that attention should be paid to different cell line metabolic demands when
317 considering optimal size for recapitulation of hepatic O_2 . Moreover, the HepaRG cell line is
318 potentially more relevant for optimisation since these spheroids do not proliferate once
319 differentiated and more closely resemble *in vivo* functionality (Gunness et al., 2013).

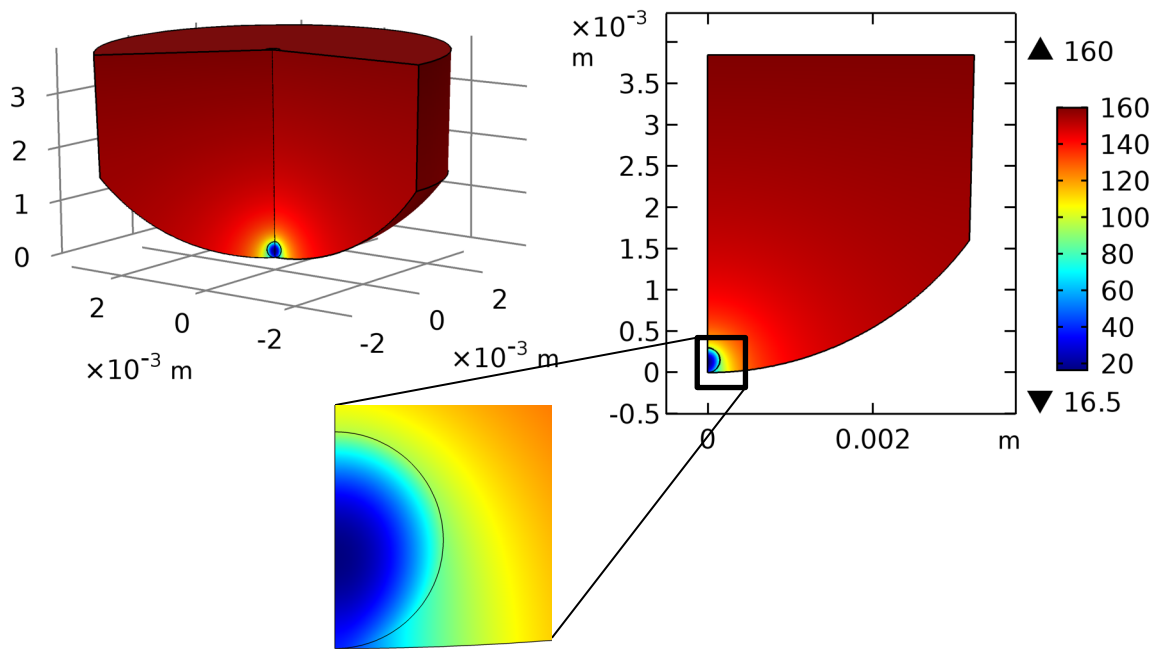
320 ***3.2 Model II: Recapitulation of the in vivo sinusoid gradient within a representative in*** 321 ***vitro environment***

322 Model II adopts radial symmetry in cylindrical coordinates, with the central vertical axis of the
323 well (top-to-bottom) representing the central axis of symmetry, and takes into account the
324 diffusion of oxygen through the media as well as inside the hepatocytes as before. The output
325 of Model II differs to Model I in two key ways. Firstly, the oxygen concentration at the
326 boundary of the spheroid is no longer explicitly specified and imposed as a constant value, but
327 rather depends on the concentration at the media-air interface (atmosphere) and subsequent
328 dynamic effects of diffusion through the media, flux into the spheroid and consumption within
329 the spheroid. Secondly, the spatial oxygen dynamics within the spheroid are no longer
330 symmetrical about the centre of the spheroid due to the position of the spheroid within the well

331 and the location of the oxygen source, at the top of the well (Figure 5). This asymmetric
332 distribution of oxygen concentration is supported experimentally by observed distributions of
333 hypoxia within spheroids in culture (e.g., see hypoxic FaDu spheroid in Figure 6C). By
334 quantifying regions of hypoxia using relative light units, it is clear that more hypoxic conditions
335 are observed towards the bottom of the *in vitro* spheroid (Figure 6D-E). The asymmetry within
336 the hepatic spheroid of the *in silico* model can be visualised more clearly by a 1D representation
337 of the spatial oxygen dynamics through a central axis of symmetry cross-section (Figure 6A-
338 B). It is clear from this representation that the minimum oxygen concentration is not found at
339 the centre of the spheroid but at a distance closer to the bottom of the well. For example, under
340 the modelling conditions of a HepaRG spheroid of radius 150 μm in 100 μl of media, the
341 minimum oxygen concentration is predicted to be approximately 16 mmHg at 129 μm from

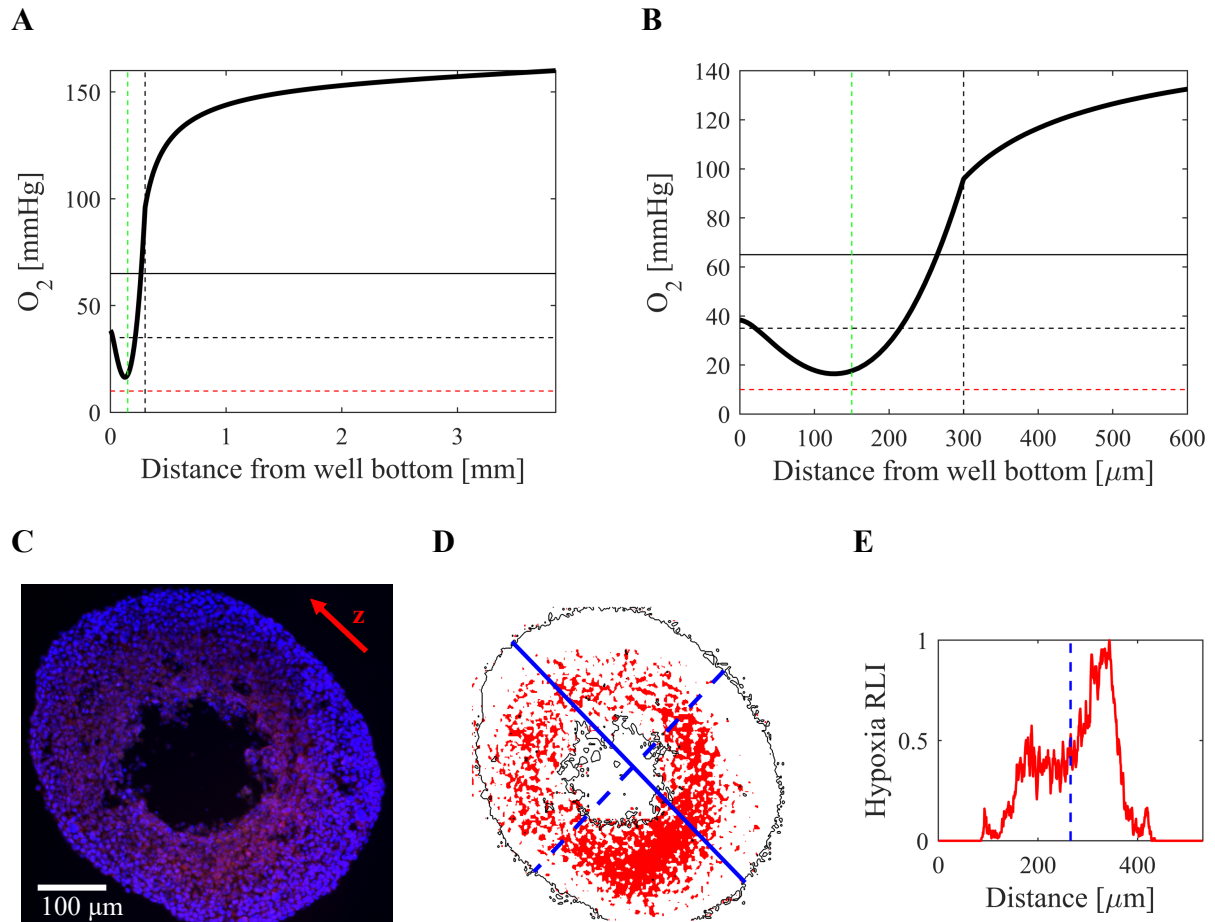
342 the bottom of the well (i.e., $\sim 20 \mu\text{m}$ away from the core, at the distal side of the spheroid,
343 relative to the oxygen source).

344



345

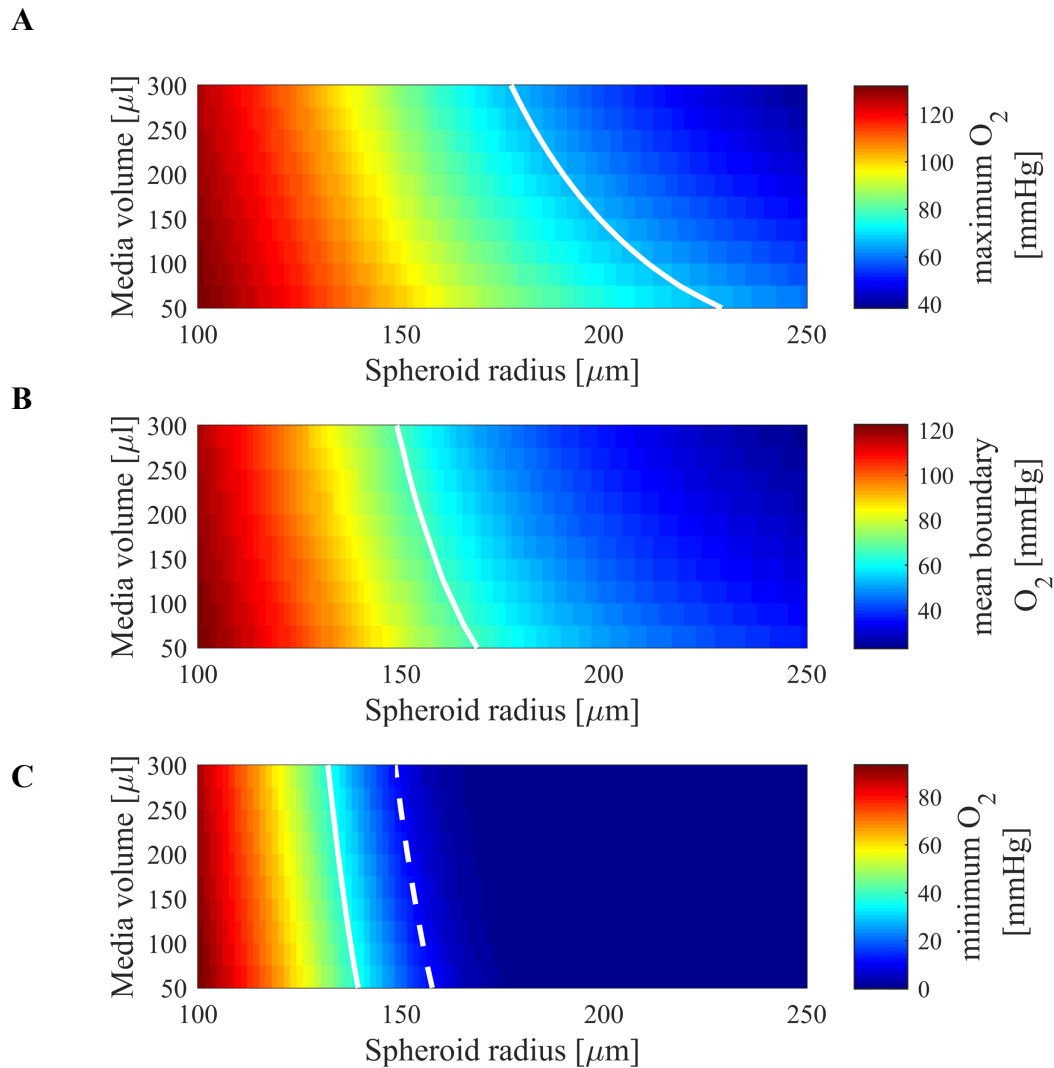
346 **Figure 5: Simulated 3D spatial oxygen dynamics within the *in vitro* culture environment.**
347 Model II simulation results for a geometrically relevant environment to represent the spatial
348 distribution of oxygen concentration for hepatic spheroids cultured *in vitro*. The model output
349 represents the steady state solution for a HepaRG spheroid of radius $150 \mu\text{m}$ in $100 \mu\text{l}$ of media.
350 The results can be visualised in 2D due to the axisymmetric nature of the problem and the
351 region containing the hepatic spheroid is highlighted for clarity.
352



354 **Figure 6: 1D cross-section of spatial oxygen dynamics.** (A): 1D cross-section of the model
 355 simulation described in Figure 5 with respect to the axisymmetric z-axis (represented as
 356 distance from the bottom of the well). (B): The same results are plotted for a reduced spatial
 357 range to visualise oxygen dynamics within the spheroid more clearly. Solid and dashed
 358 horizontal black lines indicate desired oxygen concentrations for periportal and perivenous
 359 zones within the liver. Horizontal red dashed lines represent the threshold for hypoxia. Vertical
 360 green dashed lines represent the centre of the spheroid. Vertical black dashed lines represent
 361 the spheroid boundary. (C): Example of an *in vitro* spheroid exhibiting asymmetrical oxygen
 362 distribution. Image represents immunohistochemical staining of a hypoxic FaDu spheroid with
 363 cell nuclei indicated in blue and hypoxia in red. The red arrow indicates a representative z-axis.
 364 (D): Spatial plot of the relative light intensity (RLI) of hypoxia within the spheroid. Blue lines
 365 indicate the representative z-axis relative to the bottom of the well (solid) and a cross-section
 366 through the centre of the spheroid (dashed, for comparison with (E)). (E): Hypoxia RLI versus
 367 distance from the top of the spheroid. RLI (red) is calculated for each position along the z- axis
 368 from the top to the bottom of the spheroid. The spheroid centre is also indicated (blue dashed
 369 line).
 370

371 Ideally, in order to optimise the *in vitro* system to be more representative of the hepatic oxygen
 372 range observed *in vivo*, the maximum oxygen concentration within the spheroid would

373 correspond to that in the periportal blood and the minimum oxygen concentration would
374 correspond to that in the perivenous blood. One experimentally convenient method to vary the
375 local oxygen concentration experienced by the spheroid is to adjust the media volume. Thus,
376 the identification of optimal conditions for replicating the desired oxygen gradient can be
377 investigated by comparing variations in both media volume and spheroid radius. By calculating
378 the steady state solutions of Model II for a relevant range of media volumes (50-300 μl) and
379 spheroid radii (100-250 μm), the oxygen concentrations at specific locations within the
380 geometry can be compared for optimisation (Figure 7). The two primary quantities of interest
381 are the maximum oxygen value at the spheroid boundary (Figure 7A) and the minimum
382 concentration within the spheroid (Figure 7C). We also calculate an average oxygen value
383 (Figure 7B) in acknowledgement of the heterogeneity across the boundary (e.g., see Figure 5).
384 Spheroid-radius/media-volume parameter combinations are optimised by identifying the
385 values that provide the desired oxygen concentration in each region, indicated by solid white
386 contours in Figure 7. A dashed white contour in Figure 7B also denotes at which radii/volume
387 hypoxia is predicted to occur within the spheroid. The variation in oxygen concentrations
388 appears to be more significant with spheroid radius rather than media volume, and so this
389 parameter is deemed more sensitive within these relevant physical ranges.



390 **Figure 7: Identification of *in vivo* oxygen concentrations for different *in vitro* culture**
 391 **conditions in two distinct spheroid regions.** Steady state oxygen concentrations are
 392 calculated for a range of spheroid radii and media volumes representing the maximum (A) and
 393 average (B) spheroid boundary values, and the minimum values within the spheroid (C). Solid
 394 white contours represent the curve along which the oxygen concentration is equal to the desired
 395 *in vivo* value for periportal (A, B) and perivenous (C) regions. The dashed white contour
 396 indicates which spheroid radius and media volume combinations lead to hypoxia within the
 397 spheroid as predicted by the mathematical model.
 398

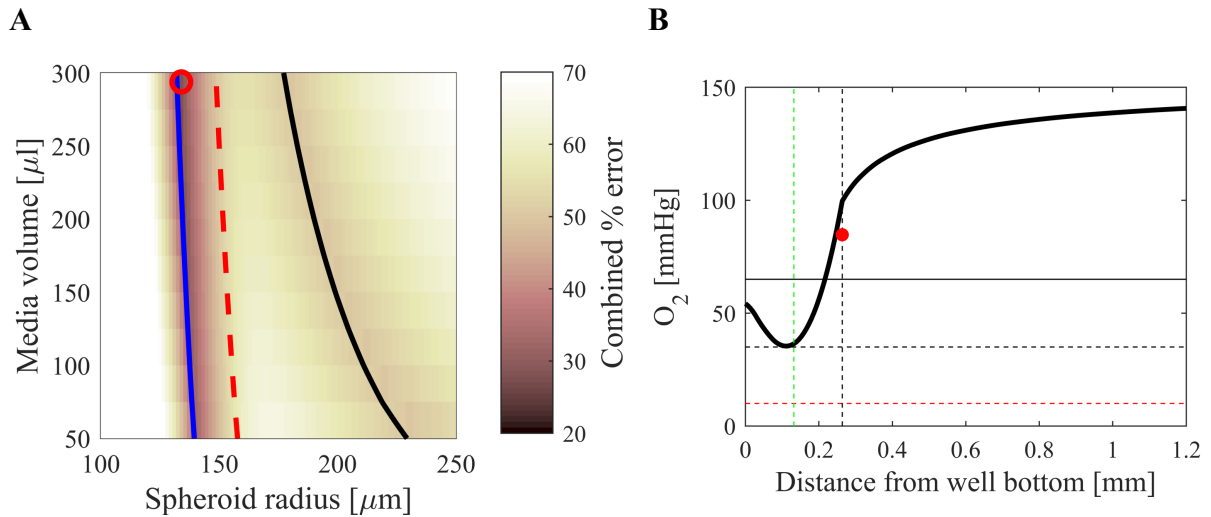
399 For a given spheroid radius, the mathematical model can suggest what amount of media volume
 400 leads to physiologically relevant oxygen concentrations at the boundary and at the minimum.
 401 However, it should be noted that the two optimal contours provided in Figure 7 do not intersect
 402 within the relevant ranges of radius and volume parameters. This is more clearly indicated in

403 Figure 8, where the contours are collated onto the same plot. Therefore, in order to optimise
 404 the *in vitro* system within these physical ranges, it is not possible to simultaneously satisfy both
 405 conditions for the desired *in vivo* gradient, and thus an intermediate region in parameter space
 406 must be identified which optimally satisfies the problem with minimum error. The percentage
 407 error associated with each combination of spheroid radius and media volume is calculated by
 408 combining the absolute differences at both the maximal spheroid boundary and minimum
 409 oxygen value within the spheroid according to the following formula:

$$\text{Combined \% error} = \frac{1}{2} \left(\frac{|C_{max} - C_{PV}|}{C_{PV}} + \frac{|C_{min} - C_{CV}|}{C_{CV}} \right) \times 100 \quad (9)$$

410 This error is plotted across the parameter space in Figure 8A and the minimum error can
 411 subsequently be identified, corresponding to a spheroid of radius 131.82 μm and media volume
 412 of 300 μl . The 1D oxygen profile for this parameterisation can be seen in Figure 8B. Note that
 413 even a significant increase in media volume yields little improvement in the minimisation of
 414 the combined % error (e.g., a media volume of 600 μl , with spheroid radius of 127.27 μm ,
 415 decreases the error from 27.2% to 23.6%, and the contours do not intersect for media volumes
 416 up to 5×10^4 μl – data not shown). In Figure 8B, the compromised oxygen gradient can be
 417 clearly visualised whereby the minimal oxygen concentration is optimal and well above the
 418 hypoxic threshold, but the maximal, and even the average oxygen concentration around the
 419 spheroid boundary (indicated in red), are above the desired periportal value. Nevertheless, these
 420 optimal values provide a range of oxygen values which encompass the desired sinusoid
 421 gradient. However, analysis of the sensitivity of the model discrepancy to perturbations in these
 422 optimal parameters reveals that the HepaRG spheroid is a sensitive system, with a 20%
 423 decrease in the spheroid radius (~ 105 μm) leading to a +69% average error in the optimal
 424 oxygen values and a 20% increase in the spheroid radius (~ 158 μm) resulting in a -57% average

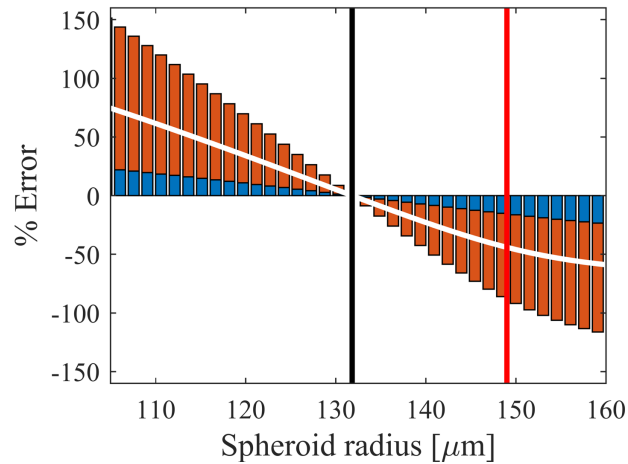
425 error (Figure 9). Furthermore, it should be noted that, in this scenario, the model predicts that
 426 an increase in radius of just 17.18 μm (or measurement error of 17.18 μm) will lead to the onset
 427 of hypoxia within the spheroid.



428

429 **Figure 8: Error calculation and minimisation in order to identify overall optimal *in vitro***
 430 **culture conditions.** (A): Figure 7 contours for the optimal conditions that provide desired
 431 maximum spheroid oxygen concentration (solid, black), minimum spheroid oxygen
 432 concentration (solid, blue) and hypoxia (dashed, red) are collated onto a single plot. This plot
 433 shows the overall optimal operating conditions for the relevant ranges of spheroid radii and
 434 media volume through the calculation of a combined % error. The minimum error is indicated
 435 by a red circle. Note that in order to prevent hypoxia, the operating conditions should lie to the
 436 left of the hypoxic threshold. (B): The 1D oxygen profile corresponding to the minimum error
 437 parametrisation (red circle, (A)), is plotted with the same format and annotations as in Figure
 438 6. The red dot indicates the average spheroid boundary concentration around the entire
 439 spheroid.

440



441

442 **Figure 9: Error sensitivity analysis of the optimal operating conditions proposed by Model**
 443 **II for HepG2 spheroids.** The percentage error for both the minimum oxygen concentration
 444 (red) and the maximum boundary concentration (blue) in the spheroid are plotted for variations
 445 in the optimal spheroid radius (131.82 μm) in 300 μl of media. An average error is also
 446 indicated (white line). The optimal spheroid radius to recapitulate the oxygen gradient (black
 447 line) and radius threshold for hypoxia (red line) are also shown.
 448

449 **4 Discussion**

450 Optimisation of the *in vitro* hepatic spheroid system requires that culture conditions are
 451 calibrated such that physiologically relevant oxygen ranges are established. Mathematical
 452 models provide a means of testing the system in order to optimise physical system parameters
 453 in order to obtain desired system properties and consequently guide the process of 3D *in vitro*
 454 study design. Specifically, a model that is properly parameterised for intrinsic physiological
 455 processes (e.g. oxygen consumption rate, diffusion rate of oxygen) can be used to identify and
 456 optimise parameters such as media volume or spheroid radius that lead to the establishment of
 457 the *in vivo*-like hepatic sinusoid oxygen gradient. Consequently, such *in silico* models directly
 458 inform the design of experiments aiming to reproduce liver physiology *in vitro*.

459 Several insightful results regarding the optimal culture conditions have been acquired through
 460 the development and analysis of two mechanistic mathematical models, parameterised using
 461 experimental data. Provided one could ensure the fixed physiological oxygen concentration at

462 the spheroid boundary, Model I predicts that sinusoid gradients can be achieved for HepaRG
463 and HepG2 spheroids of radii 100 μm and 170 μm respectively (with the onset of hypoxia
464 occurring at 142 μm and 241 μm). HepG2 spheroids can afford to grow to a larger size without
465 experiencing hypoxia due to the reduced demand for oxygen (lower oxygen consumption rate,
466 V_{max}). This lower demand in oxygen may be due to the finding that in their unstressed state,
467 HepG2 cells produce cellular energy from both oxidative phosphorylation and anaerobic
468 glycolysis, due to the Warburg effect, and thus a reduced oxygen consumption rate is measured
469 due to the additional production of ATP via glycolysis (Kamalian et al., 2018). Conversely,
470 HepaRG cells only produce ATP via oxidative phosphorylation in the unstressed state and so
471 would need to consume more oxygen to produce the same amount of ATP. However, Model I
472 assumes the spheroid is cultured in a 3D radially symmetric environment whereas this
473 assumption is not valid in most experimental models. The extension of Model II to a more
474 realistic well geometry means that the precise end-points of the *in vivo* sinusoid gradient cannot
475 simultaneously be satisfied for any given combination of spheroid radius and media depth
476 combination. Therefore, culture conditions are identified by the model that minimise the
477 potential error of the end-points at the average spheroid boundary and minimum oxygen value
478 within the spheroid. This optimisation corresponds to a HepaRG spheroid radius of 132 μm
479 (with a revised hypoxic threshold of 149 μm) and 300 μl of media volume, which is in contrast
480 with more common instructions for culturing spheroids in 100 μl media (Korff, 2004, Charoen
481 et al., 2014, Morrison et al., 2016). However, the model oxygen gradient is more sensitive to
482 the spheroid radius parameter, and thus careful consideration should be given for spheroids that
483 change size over the defined culture period. In particular, sensitivity analysis reveals that small
484 perturbations in spheroid radius can lead to larger average errors in the gradient, relative to the
485 perturbation, and therefore precision is required to avoid the onset of hypoxia while preserving
486 central vein values. The application of both Models I and II suggest that there is a difference

487 in predicted optimal spheroid size when you take into account well geometry and oxygen
488 diffusion through the media.

489 Another cell culture system currently used within the field comprises a multi-well plate with a
490 gas-permeable bottom, covered with agarose to form U-shaped layer. This system is designed
491 to improve the delivery of oxygen to multicellular spheroids and prevent necrosis in the centre
492 of the spheroid. This feature, in combination with a U-shaped agarose layer, could alleviate the
493 asymmetry of the oxygen profile in ULA plates. This alternative system was therefore
494 implemented within our mathematical modelling framework by replicating the geometry for
495 Model II with the further addition of 100 μl of agarose to form a U-shaped layer with a flat,
496 gas-permeable bottom at the bottom of the well (for details of the investigation, see
497 Supplementary Material). The results of this study (complementary to that of the ULA plate)
498 showed that indeed, while symmetry was improved and larger non-hypoxic spheroids could be
499 cultured, it was still not possible to achieve the desired *in vivo* gradient exactly. Model analysis
500 identified a desired central oxygen concentration of 35 mmHg for an optimised 145.45 μm
501 radius spheroid in 300 μl media. However, oxygen at the spheroid boundary, whilst relatively
502 homogenous compared with the ULA plate system, remained too high for atmospheric external
503 oxygen tensions.

504 The calibration and optimisation of intra-spheroidal oxygen profiles may also be improved via
505 the controlled regulation of oxygen tensions within a cell culture incubator. The presented work
506 has focused on the atmospheric oxygen levels commonly utilised within cell culture
507 experiments. However, these non-physiological levels could result in hyperoxia if the media
508 volume or spheroid size is insufficient (Gomes et al., 2016). Indeed, this issue can be seen for
509 such scenarios as simulated by our model (e.g., Figure 7). Additionally, the use of further
510 alternative cell culture formats may improve recapitulation of the *in vivo* sinusoid gradient in

511 hepatic spheroids. It is possible that the geometry of the hanging drop system would provide a
512 more uniform, symmetric oxygen profile; however, this system uses a very small volume of
513 liquid and so issues regarding waste products, medium changes and tight control of the oxygen
514 environment must be considered. The culture of multiple small aggregates in a single well has
515 also been shown to influence the oxygen distribution and lower steady state values and could
516 therefore potentially be used as an optimisation tool (Lesher-Pérez et al., 2017).

517 Mathematical models comprise a useful tool for simulating physical problems, testing
518 hypotheses *in silico*, and guiding subsequent experimental work. However, they are inherently
519 simplified and abstract for tractability, and while driven by experimental data for calibration,
520 it is also important to acquire feedback in the form of empirical data and continue model
521 refinement. Thus, successful (i.e., useful) models (both mathematical and experimental) are the
522 result of the iterative cycle between *in silico* and *in vitro* work. This model was implemented
523 to thoroughly and efficiently analyse the physical and mechanistic conditions that influence
524 spatial oxygen distribution in hepatic spheroids in view of commonly practised cell culture
525 methodologies. The model simulates outputs that are inefficient and difficult to
526 comprehensively obtain *in vitro*, but would now benefit from testing and verification
527 experiments including local, real-time measurements of oxygen and evidence of hypoxic levels
528 within the spheroid under specified scenarios.

529 Many previous *in silico* models have focused on oxygen kinetics in spheroids, highlighting the
530 importance of properly characterising these mechanisms that describe the underlying
531 biophysical processes. Most of these models rely on symmetrical properties or biochemical
532 parameters derived from tumour spheroids. Such modelling work covers a range of applications
533 that ultimately emphasise the need for optimisation of these *in vitro* systems, whether through
534 the optimisation of spheroid morphology (Leung et al., 2015), defining optimal spheroid
535 viability and functionality (Glicklis et al., 2004), or accounting for perfusion velocity and flow

536 within microbio reactors (Allen & Bhatia, 2003, Hu & Li, 2007, Barisam et al., 2018). Some
537 key novelties arising from our multidisciplinary modelling work include the measurement of
538 oxygen uptake parameters that are integrated into mathematical models to generate bespoke
539 dynamics for both HepG2 and HepaRG cell lines; the development and parameterisation of a
540 model that takes into account a realistic ULA geometry with, most importantly, asymmetry;
541 and an improved guide for media volume conditions in these environments relevant to hepatic
542 spheroid culture. The utility of this spheroid mathematical modelling framework can be further
543 extended to incorporate drug transport and metabolism components in a similar approach,
544 ultimately providing a more realistic description of the environment and culturing conditions
545 used *in vitro* for improved medical applications.

546 **Acknowledgements**

547 The work was supported by the National Centre for the Replacement, Refinement and
548 Reduction of Animals in Research (NC3Rs) CRACK-IT fund, Challenge 5: IVIVE. JL, RNB
549 and SDW acknowledge funding support from the Liverpool Centre for Mathematics in
550 Healthcare (EPSRC grant: EP/N014499/1). JL is supported by an MRC Skills Development
551 Fellowship (MR/S019332/1).

552 **Author contributions**

553 JL wrote the manuscript; JL, RNB & SDW contributed to the mathematical modelling; AEC,
554 HEC & CM contributed to the experimental inputs; HG, DPW & SDW designed the research.
555 SDW directed the research. All authors read and approved the final manuscript.

556 **Declaration of interests**

557 The authors declare that they have no competing interests.

558 **References**

559 Allen J W and Bhatia S N (2003) Formation of steady-state oxygen gradients in vitro:
560 Application to liver zonation. *Biotechnology and bioengineering* 82: 253-262.

561
562 Anada T, Fukuda J, Sai Y and Suzuki O (2012) An oxygen-permeable spheroid culture system
563 for the prevention of central hypoxia and necrosis of spheroids. *Biomaterials* 33: 8430-8441.

564
565 Barisam M, Saidi M S, Kashaninejad N and Nguyen N-T (2018) Prediction of Necrotic Core
566 and Hypoxic Zone of Multicellular Spheroids in a Microbioreactor with a U-Shaped Barrier.
567 *Micromachines* 9: 94.

568
569 Brown J M and Giaccia A J (1998) The unique physiology of solid tumors: opportunities (and
570 problems) for cancer therapy. *Cancer research* 58: 1408-1416.

571
572 Buerk D G and Sidel G M (1978) Local kinetics of oxygen metabolism in brain and liver
573 tissues. *Microvascular research* 16: 391-405.

574
575 Carmeliet P and Jain R K (2000) Angiogenesis in cancer and other diseases. *nature* 407: 249.

576
577 Carreau A, Hafny-Rahbi B E, Matejuk A, Grillon C and Kieda C (2011) Why is the partial
578 oxygen pressure of human tissues a crucial parameter? Small molecules and hypoxia. *Journal*
579 *of cellular and molecular medicine* 15: 1239-1253.

580
581 Chaplain M (1996) Avascular growth, angiogenesis and vascular growth in solid tumours: The
582 mathematical modelling of the stages of tumour development. *Mathematical and computer*
583 *modelling* 23: 47-87.

584
585 Charoen K M, Fallica B, Colson Y L, Zaman M H and Grinstaff M W (2014) Embedded
586 multicellular spheroids as a biomimetic 3D cancer model for evaluating drug and drug-device
587 combinations. *Biomaterials* 35: 2264-2271.

588
589 Colley H E, Hearnden V, Avila-Olias M, Cecchin D, Canton I, Madsen J, MacNeil S, Warren
590 N, Hu K and McKeating J A (2014) Polymersome-mediated delivery of combination anticancer
591 therapy to head and neck cancer cells: 2D and 3D in vitro evaluation. *Molecular pharmaceutics*
592 11: 1176-1188.

593
594 Colton C K (1995) Implantable biohybrid artificial organs. *Cell transplantation* 4: 415-436.

595
596 Corning Life Sciences. (2018). "Life Sciences Products and Equipment." Retrieved 8 Oct,
597 2018, from <http://www.corning.com/lifesciences/>.

598
599 Curcio E, Salerno S, Barbieri G, De Bartolo L, Drioli E and Bader A (2007) Mass transfer and
600 metabolic reactions in hepatocyte spheroids cultured in rotating wall gas-permeable membrane
601 system. *Biomaterials* 28: 5487-5497.

602
603 Foy B D, Rotem A, Toner M, Tompkins R G and Yarmush M L (1994) A device to measure
604 the oxygen uptake rate of attached cells: importance in bioartificial organ design. *Cell*
605 *Transplantation* 3: 515-527.

606
607 Freyer J P (1988) Role of necrosis in regulating the growth saturation of multicellular
608 spheroids. *Cancer research* 48: 2432-2439.

609
610 Glicklis R, Merchuk J C and Cohen S (2004) Modeling mass transfer in hepatocyte spheroids
611 via cell viability, spheroid size, and hepatocellular functions. *Biotechnology and*
612 *bioengineering* 86: 672-680.

613
614 Gomes A, Guillaume L, Grimes D R, Fehrenbach J, Lobjois V and Ducommun B (2016)
615 Oxygen partial pressure is a rate-limiting parameter for cell proliferation in 3d spheroids grown
616 in physioxic culture condition. *PloS one* 11: e0161239.

617
618 Grimes D R, Kelly C, Bloch K and Partridge M (2014a) A method for estimating the oxygen
619 consumption rate in multicellular tumour spheroids. *J R Soc Interface* 11: 20131124.

620
621 Grimes D R, Fletcher A G and Partridge M (2014b) Oxygen consumption dynamics in steady-
622 state tumour models. *Royal Society Open Science* 1: 140080.

623
624 Grimes D R, Kannan P, McIntyre A, Kavanagh A, Siddiky A, Wigfield S, Harris A and
625 Partridge M (2016) The role of oxygen in avascular tumor growth. *PloS one* 11: e0153692.

626
627 Gunness P, Mueller D, Shevchenko V, Heinzle E, Ingelman-Sundberg M and Noor F (2013)
628 3D organotypic cultures of human HepaRG cells: a tool for in vitro toxicity studies.
629 *Toxicological sciences* 133: 67-78.

630
631 Hu G and Li D (2007) Three-dimensional modeling of transport of nutrients for multicellular
632 tumor spheroid culture in a microchannel. *Biomedical microdevices* 9: 315-323.

633
634 Jungermann K and Keitzmann T (1996) Zonation of parenchymal and nonparenchymal
635 metabolism in liver. *Annual review of nutrition* 16: 179-203.

636
637 Jungermann K and Kietzmann T (2000) Oxygen: modulator of metabolic zonation and disease
638 of the liver. *Hepatology* 31: 255-260.

639
640 Kamalian L, Douglas O, Jolly C E, Snoeys J, Simic D, Monshouwer M, Williams D P, Park B
641 K and Chadwick A E (2018) The utility of HepaRG cells for bioenergetic investigation and
642 detection of drug-induced mitochondrial toxicity. *Toxicology in Vitro* 53: 136-147.

643
644 Kietzmann T (2017) Metabolic zonation of the liver: The oxygen gradient revisited. *Redox*
645 *biology* 11: 622-630.

646
647 Korff T (2004). Three-dimensional in vitro angiogenesis assays. Methods in Endothelial Cell
648 Biology, Springer: 115-123.

649
650 Kyffin J A, Sharma P, Leedale J, Colley H E, Murdoch C, Mistry P and Webb S D (2018)
651 Impact of cell types and culture methods on the functionality of in vitro liver systems-A review
652 of cell systems for hepatotoxicity assessment. *Toxicology In Vitro* 48: 262-275.

653
654 Lee-Montiel F T, George S M, Gough A H, Sharma A D, Wu J, DeBiasio R, Verneti L A and
655 Taylor D L (2017) Control of oxygen tension recapitulates zone-specific functions in human
656 liver microphysiology systems. *Experimental Biology and Medicine* 242: 1617-1632.

657
658 Lee S H, Do S-I and Kim H-S (2014) Hyperoxia accelerates progression of hepatic fibrosis by
659 up-regulation of transforming growth factor- β expression. *World Journal of Gastroenterology*:
660 *WJG* 20: 3011.

661
662 Leedale J, Herrmann A, Bagnall J, Fercher A, Papkovsky D, Sée V and Bearon R N (2014)
663 Modeling the dynamics of hypoxia inducible factor-1 α (HIF-1 α) within single cells and 3D cell
664 culture systems. *Mathematical biosciences* 258: 33-43.

665
666 Leshner-Pérez S C, Kim G-A, Kuo C-h, Leung B M, Mong S, Kojima T, Moraes C, Thouless
667 M, Luker G D and Takayama S (2017) Dispersible oxygen microsensors map oxygen gradients
668 in three-dimensional cell cultures. *Biomaterials science* 5: 2106-2113.

669
670 Leung B M, Leshner-Perez S C, Matsuoka T, Moraes C and Takayama S (2015) Media additives
671 to promote spheroid circularity and compactness in hanging drop platform. *Biomaterials*
672 *science* 3: 336-344.

673
674 Lodish H, Berk A, Zipursky S L, Matsudaira P, Baltimore D and Darnell J (2000). Molecular
675 cell biology, WH Freeman New York.

676
677 Martinez I, Nedredal G I, Øie C I, Warren A, Johansen O, Le Couteur D G and Smedsrød B
678 (2008) The influence of oxygen tension on the structure and function of isolated liver sinusoidal
679 endothelial cells. *Comparative hepatology* 7: 4.

680

681 Mattei G, Magliaro C, Giusti S, Ramachandran S D, Heinz S, Braspenning J and Ahluwalia A
682 (2017) On the adhesion-cohesion balance and oxygen consumption characteristics of liver
683 organoids. *PloS one* 12: e0173206.

684
685 Mehta G, Hsiao A Y, Ingram M, Luker G D and Takayama S (2012) Opportunities and
686 challenges for use of tumor spheroids as models to test drug delivery and efficacy. *Journal of*
687 *Controlled Release* 164: 192-204.

688
689 Morrison E, Wai P, Leonidou A, Bland P, Khalique S, Farnie G, Daley F, Peck B and Natrajan
690 R (2016) Utilizing functional genomics screening to identify potentially novel drug targets in
691 cancer cell spheroid cultures. *Journal of visualized experiments: JoVE*.

692
693 Muz B, de la Puente P, Azab F and Azab A K (2015) The role of hypoxia in cancer progression,
694 angiogenesis, metastasis, and resistance to therapy. *Hypoxia* 3: 83.

695
696 Nyberg S L, Remmel R P, Mann H J, Peshwa M V, Hu W-S and Cerra F B (1994) Primary
697 hepatocytes outperform Hep G2 cells as the source of biotransformation functions in a
698 bioartificial liver. *Annals of surgery* 220: 59.

699
700 Olive P L, Vikse C and Trotter M J (1992) Measurement of oxygen diffusion distance in tumor
701 cubes using a fluorescent hypoxia probe. *International Journal of Radiation Oncology**
702 *Biology* Physics* 22: 397-402.

703
704 Rangan S (1972) A new human cell line (FaDu) from a hypopharyngeal carcinoma. *Cancer*
705 29: 117-121.

706
707 Riffle S and Hegde R S (2017) Modeling tumor cell adaptations to hypoxia in multicellular
708 tumor spheroids. *Journal of Experimental & Clinical Cancer Research* 36: 102.

709
710 Shipley R, Davidson A J, Chan K, Chaudhuri J B, Waters S and Ellis M J (2011) A strategy to
711 determine operating parameters in tissue engineering hollow fiber bioreactors. *Biotechnology*
712 *and bioengineering* 108: 1450-1461.

713
714 Vaupel P, Kallinowski F and Okunieff P (1989) Blood flow, oxygen and nutrient supply, and
715 metabolic microenvironment of human tumors: a review. *Cancer research* 49: 6449-6465.

716
717 Ward J P and King J R (2003) Mathematical modelling of drug transport in tumour multicell
718 spheroids and monolayer cultures. *Mathematical biosciences* 181: 177-207.

719
720 Williams D P, Shipley R, Ellis M J, Webb S, Ward J, Gardner I and Creton S (2013) Novel in
721 vitro and mathematical models for the prediction of chemical toxicity. *Toxicology research* 2:
722 40-59.

- 723
724 Yamada K M and Cukierman E (2007) Modeling tissue morphogenesis and cancer in 3D. *Cell*
725 130: 601-610.
- 726
727 Yarmush M, Toner M, Dunn J, Rotem A, Hubel A and Tompkins R (1992) Hepatic tissue
728 engineering: Development of critical technologies. *Annals of the New York Academy of*
729 *Sciences* 665: 238-252.
- 730
731